Supplementary Material

1 Supplementary Data: fNIRS-EEG guided tES approach based on published dataset

Published dataset is based on the research protocol was approved by the All India Institute of Medical Sciences, New Delhi, India Institutional Review Board (IEC-129/07.04.2017). This current study extends our prior work (Rezaee et al., 2021) on fNIRS-EEG joint imaging (Guhathakurta and Dutta, 2016) of ctDCS-modulated PFC responses (Rezaee et al., 2021) by investigating cortical activation using AtlasViewer toolbox (Aasted et al., 2015). This fNIRS-EEG joint imaging approach can also be used for functional neuroimaging of cue reactivity in CUD (Schacht et al., 2013). Since we did not have fNIRS-EEG joint imaging data of cue reactivity in CUD, so we illustrate our fNIRS-EEG joint imaging approach to response inhibition during a virtual reality (VR)-based Balance Training (VBaT) (Rezaee et al., 2021). Figure 4 shows the computational pipeline (Guhathakurta and Dutta, 2016) where AtlasViewer toolbox (Aasted et al., 2015) was used to conduct a Monte Carlo simulation that provided a forward matrix representing each channel's spatial sensitivity profile to cortical absorption changes, i.e., the fNIRS sensitivity profile. The forward matrix, F, transformed from the voxel space of localized changes, X, to the optode measurement space, Y, i.e., $Y = FX$. The X for image reconstruction can be obtained by solving the inverse problem (Rytov approximation (Devaney, 1981)) using AtlasViewer toolbox (Aasted et al., 2015) in Matlab (Mathworks, Inc., USA), i.e., $X = F^T(FF^T + \alpha I)^{-1}Y$, where I is the identity matrix and α is the regularization parameter (=0.01). Here, Y is the post-ctDCS change in the canonical scores of O2Hb concentration from pre-tDCS baseline. The Monte-Carlo simulation was set up with 100 million photons being injected by each source using the default optical parameters for each layer of the head model. Then, based on the PFC activation during response inhibition in VBaT, a fully automated pipeline – realistic volumetric-approach to simulate transcranial electric stimulation (ROAST) version 3 (Huang et al., 2017) – was used to find the tES electrode placement for targeting the brain activation found from image reconstruction using AtlasViewer toolbox (Aasted et al., 2015) in Matlab (Mathworks, Inc., USA). Different optimization criteria, including maximal-intensity and maximal-focality, can be used in the Matlab (Mathworks, Inc., USA) function called "roast_target" based on a lead-field matrix from an individualized (MRI-based) head model. In this study, we used maximal-focality optimization criteria to target the response inhibition brain activation with 4x1 high-definition (HD) tDCS montage (Mikkonen et al., 2020).

2 Supplementary Figures: neuroimaging guided NIBS in cannabis use disorder

CLOS pipeline uses structural magnetic resonance images (MRI) images (T1, T2) to create an anatomically accurate subject-specific head model that can be used for computing electric field distribution in the brain for a given electrode or coil location. CLOS pipeline uses freely available computational packages (simNIBS (Saturnino et al., 2018), ROAST (Huang et al., 2017)) along with freely available brain atlases (AAL (Rolls et al., 2020, 3), SUIT (Diedrichsen, 2006)) for a leadfield based approach to optimize (convex optimization (Boyd and Vandenberghe, 2004)) the electrodes or TMS coil location. The optimization is based on the quasi-uniform assumption that the local polarization effect is proportional to the local electric field strength (Bikson et al., 2013). If we consider a set of N bipolar electrodes or TMS coil locations, then the quasi-stationary Ohmic relation from the stimulation array, s, to the average electric field at a certain brain location, $\vec{\boldsymbol{E}}$, can be written in a matrix form, $\vec{\boldsymbol{E}} = \overrightarrow{\boldsymbol{LF}} \cdot s$, where $\overrightarrow{\boldsymbol{LF}}$ is the leadfield. One way to write the objective function for least squares fitting of an unknown stimulation array, x, viz. $\arg\min_x \|\overrightarrow{\boldsymbol{LF}} \cdot x - \vec{\boldsymbol{E}}\|^2$, is to minimize the L2-norm of the error, $(\overrightarrow{\boldsymbol{LF}}.x - \vec{\boldsymbol{b}})$, given a desired electric field distribution, $\vec{\boldsymbol{E}}$, e.g., to target the Purkinje cells of Crus

I/II in the fronto-cerebellar circuits (ROGERS et al., 2011). Here, it is important to limit the TMS generated electric field to the Purkinje cells in the Crus II to target for DLPFC executive network (Krienen and Buckner, 2009), which was achieved with cerebellar region-specific electric field modeling (Rezaee and Dutta, 2019) and neurophysiological validation (Batsikadze et al., 2019). Spill-over of TMS generated electric field to the dentate nuclei (DN) at higher TMS intensities will affect the recruitment curve (from inhibition to facilitation of the cerebellar-brain connection).

2.1 Supplementary Figures

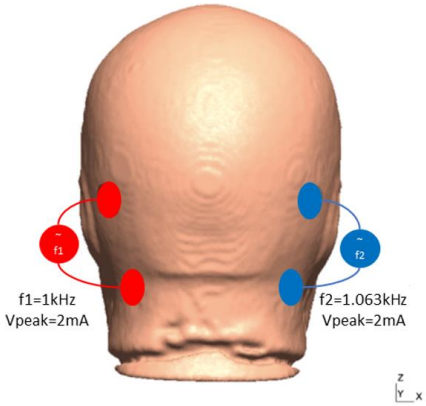

Supplementary Figure S1: An illustrative picture of transcranial temporal interference stimulation (tTIS) approach where two tACS sources with frequencies f1=1kHz and f2=1.063kHz are combined for amplitude modulation at 0.063kHz at the deep cerebellar nuclei (DCN).

At any region of the brain atlas, based on the leadfield (Rezaee and Dutta, 2019), the mean electric field ($\overrightarrow{E}$ = $\overrightarrow{LF}$ · s) can be written as vector summation, $\vec{E}$ = $\overrightarrow{LF\_PO9h}$ · PO9h + $\overrightarrow{LF\_PO10h}$ · PO10h+ $\overrightarrow{LF\_Exx7}$ · Exx7+ $\overrightarrow{LF\_Exx8}$ · Exx8. Leadfield for the cerebellar lobules from the brain atlas (AAL (Rolls et al., 2020, 3), SUIT (Diedrichsen, 2006)) given below,

Cerebellar lobules:
1. 'Left I_IV'
2. 'Right I_IV'
3. 'Left V'
4. 'Right V'
5. 'Left VI'
6. 'Vermis VI'
7. 'Right VI'
8. 'Left Crus I'
9. 'Vermis Crus I'
10. 'Right Crus I'
11. 'Left Crus II'
12. 'Vermis Crus II'
13. 'Right Crus II'
14. 'Left VIIb'
15. 'Vermis VIIb'
16. 'Right VIIb'
17. 'Left VIIIa'
18. 'Vermis VIIIa'

19. 'Right VIIIa'
20. 'Left VIIIb'
21. 'Vermis VIIIb'
22. 'Right VIIIb'
23. 'Left IX'
24. 'Vermis IX'
25. 'Right IX'
26. 'Left X'
27. 'Vermis X'
28. 'Right X'
29. ‘Left Dentate Nucleus’
30. ‘Right Dentate Nucleus’

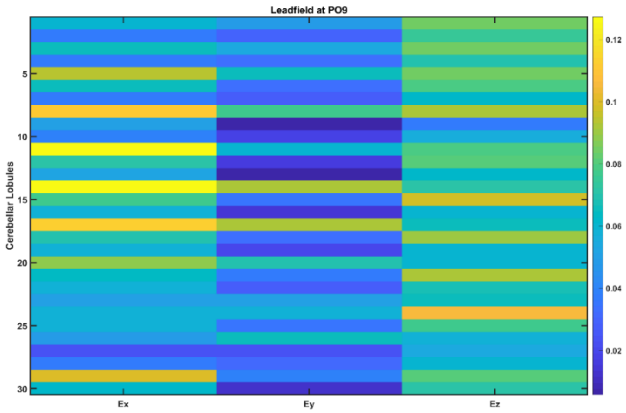

Supplementary Figure S2: Leadfield vector for PO9h at the 30 cerebellar lobules in the X, Y, and Z directions

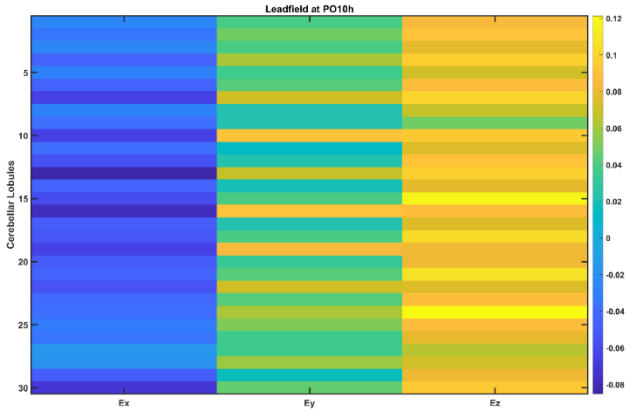

Supplementary Figure S3: Leadfield vector for PO10h at the 30 cerebellar lobules in the X, Y, and Z directions

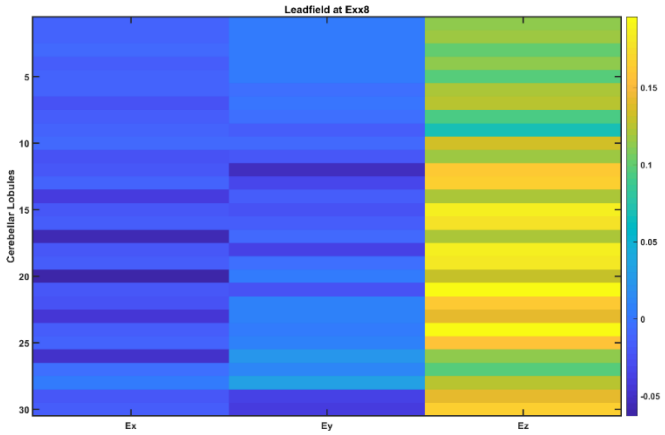

Supplementary Figure S4: Leadfield vector for Exx8 at the 30 cerebellar lobules in the X, Y, and Z directions

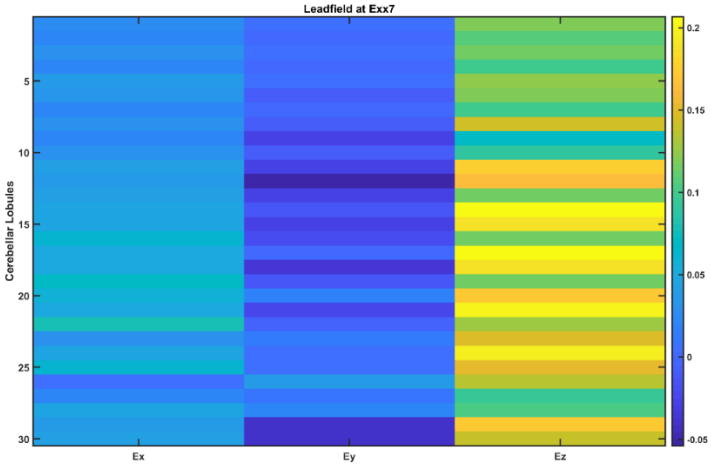

Supplementary Figure S5: Leadfield vector for Exx7 at the 30 cerebellar lobules in the X, Y, and Z directions

Circular electrodes placed at PO9h(-55.6, -70.1, -6.8) – Exx7(-54.6, -45.0, -54.0) location (shown in red in Figure S1) for tACS at 1kHz with 2mA as well PO10h(61.7, -69.7, -5.8) – Exx8(59.8, -49.3, -52.9) location (shown in blue in Figure S1) for tACS at 1.03kHz with 2mA in the X, Y, and Z directions (Figure S1). The superposition principle under Ohmic volume conductor (Leadfield approach) assumption was applied and the resultant mean electric field ($\overrightarrow{E} = \overrightarrow{LF} \cdot s$) at the cerebellar lobules are shown below.

3 Supplementary Tables and Figures: transcranial temporal interference stimulation of dentate nucleus

In our feasibility studies (Rezaee et al., 2021),(Rezaee et al., 2020), it was found challenging to optimize ctDCS electrode montage to solely stimulate the dentate nucleus without stimulating the lobes of the cerebellum (Abadi and Dutta, 2017). Therefore, we proposed this simulation study to leverage the neuronal sensitivity in transcranial temporal interference stimulation (tTIS) that depends on the neuronal membrane time-constant [84] for the dentate's focal stimulation nucleus. Here, tTIS can play

an important role in psychiatric conditions (Grossman et al., 2018) for focused modulation of deep brain structures (Lee et al., 2020) that may stimulate deeper brain regions, including anterior cingulate cortex and deep cerebellar nuclei. Based on the leadfield from our prior work on deep ctDCS (Rezaee et al., 2020), we investigated tTIS with 3.14cm^2 (1cm radius) circular electrodes placed at PO9h(-55.6, -70.1, -6.8) – Exx7(-54.6, -45.0, -54.0) location (shown in red in Figure 5) for tACS at 1kHz with 2mA peak current as well PO10h(61.7, -69.7, -5.8) – Exx8(59.8, -49.3, -52.9) location (shown in blue in Figure 5) for tACS at 1.03kHz with 2mA peak current. We will write f1=f-Δf and f2=f+Δf, and two tACS current sources as s1(t)=A · cos(f1 · t) and s2(t)=B · cos(f2 · t). At any region of the brain atlas, based on the leadfield (Rezaee and Dutta, 2019), the mean electric field ($\overrightarrow{E} = \overrightarrow{LF} \cdot$ s) can be written as vector summation, $\vec{E} = \overrightarrow{LF1} \cdot$ s1 + $\overrightarrow{LF2} \cdot$ s2. For the cerebellar cortex near tACS electrodes, either $\|\overrightarrow{LF1}\| \gg \|\overrightarrow{LF2}\|$ or $\|\overrightarrow{LF2}\| \gg \|\overrightarrow{LF1}\|$ so the peak electric field was primarily determined by the individual tACS current sources, s1(t) or s2(t), which was <0.2V/m at high frequency of 1kHz or 1.03kHz – details in the Supplementary Materials. Here, neuronal stimulus response functions (Meyer et al., 2017) play an essential role in neuromodulation (Dutta and Nitsche, 2013) as well as filtering operations (Heeger, 2017), where low pass properties of the membrane can drastically attenuate high (~kHz) tACS frequencies (Deans et al., 2007). Only stimulation frequencies below 100Hz have been found effective for neuromodulation via neuronal membrane (Deans et al., 2007).

In the cerebellum, the dentate nucleus (DN) cells are under intensive inhibitory drive from Purkinje cells (PCs), while the excitatory inputs are from mossy fiber and climbing fiber collaterals. However, the excitatory inputs from mossy fiber and the climbing fiber collaterals are not strong enough to generate the DN burst activity that is necessary to initiate motor behavior (Ishikawa et al., 2014). We postulate that tTIS may drive DN's burst activity without significantly affecting the PCs, which is a challenge with rTMS and tDCS due to PC's proximity to the scalp (Batsikadze et al., 2019). We further postulated that tTIS of the DN could be combined with tDCS of the PCs to coordinate population activities for dynamic synchronization (Shin and De Schutter, 2006) where inhibitory input will be important for the fine control of the E/I balance (Dagar et al., 2016) at the target DN neurons. We postulate NIBS based amelioration of dysrhythmia in the cortico-cerebello-thalamo-cortical (CCTC) loop as an extension to thalamocortical dysrhythmia (Schulman et al., 2011). In this study, we investigated tTIS using a CCTC loop model (Zhang and Santaniello, 2019) that considered the average firing rate of PCs and deep cerebellar neurons (DCN) as 63Hz and 56.6Hz, respectively, so for computational modeling of thalamocortical basal ganglia with cerebellum (Yousif et al., 2020), we selected f2-f1=63Hz for the amplitude modulation of DCN by tTIS (Grossman et al., 2017) – see Figure 5. At deeper brain regions distant from tACS electrodes with comparable electric fields, $\overrightarrow{LF1} \approx \overrightarrow{LF2}$ and we can write $\vec{E} = (\vec{a} + \vec{b}) \cdot \cos(f1 \cdot t) + (\vec{a} - \vec{b}) \cdot \cos(f2 \cdot t)$. Therefore, $\vec{E} = 2\vec{a} \cdot \cos(\frac{f1+f2}{2} \cdot t) \cdot \cos(\frac{f2-f1}{2} \cdot t) + 2\vec{b} \cdot \sin(\frac{f1+f2}{2} \cdot t) \cdot \sin(\frac{f2-f1}{2} \cdot t)$ where $\frac{f2-f1}{2} = \Delta f$ and $\frac{f1+f2}{2} = f$. Here, $\vec{E} = 2\vec{a} \cdot \cos(f \cdot t) \cdot \cos(\Delta f \cdot t) + 2\vec{b} \cdot \cos(p/2 - f \cdot t) \cdot \cos(p/2 - \Delta f \cdot t)$, which presents summation of two beats of Δf frequency but p/2 phase apart, where $\vec{b} \approx 0$ results in a single beats at certain deeper brain regions, i.e., $\vec{E} = 2\vec{a} \cdot \cos(f \cdot t) \cdot \cos(\Delta f \cdot t)$. Here, the tTIS beats can provide the burst stimulation of the DCN.

Based on the quasi-uniform assumption that local polarization effect is proportional to the local electric field strength (Bikson et al., 2013), the electric field modulation of the deep cerebellar nucleus (DCN) was simulated with the thalamocortical basal ganglia network with DCN model (seven first-order coupled differential equations) from (Yousif et al., 2020) – see Figure S9. Their code was available from the ModelDB website (accession number 261882). Their code parameters are for the healthy state – see below from (Yousif et al., 2020).

Connection	Weight	Polarity	Healthy state parameters
Th -> Cx	w1	+	20
Cx -> Th	w2	+	5
nRT -> Th	w3	–	8
DCN -> Th	w4	+	25
GPi -> Th	w5	–	15
Cx -> nRT	w6	+	5
STN -> GPe	w7	+	19
GPe -> GPe	w8	–	5
STN -> GPi	w9	+	15
Cx -> STN	w10	+	20
GPe -> STN	w11	–	20
ext -> DCN	ext	+	3.42

3.1 Supplementary Figures

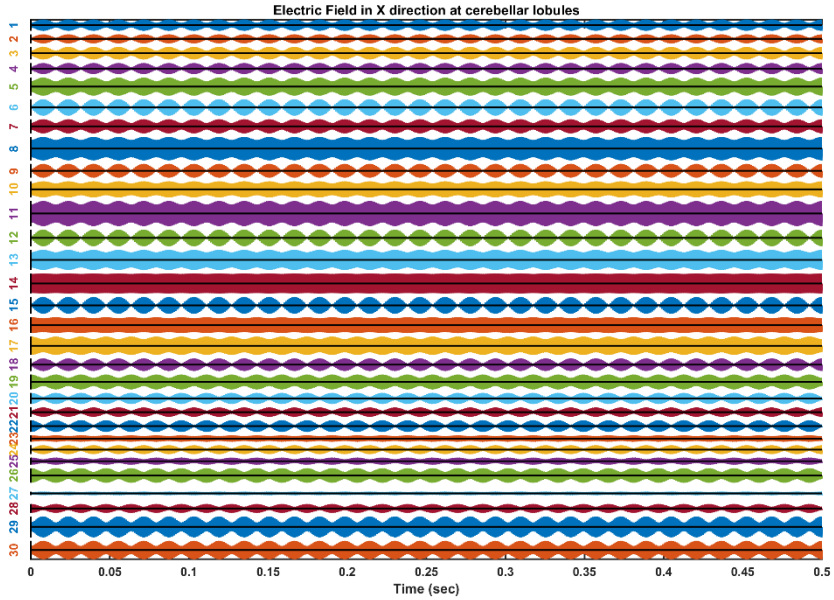

Supplementary Figure S6: tTIS - the resultant mean electric field in X direction at the cerebellar lobules shows the beats at 63Hz at the dentate nuclei (lobules 29 and 30)

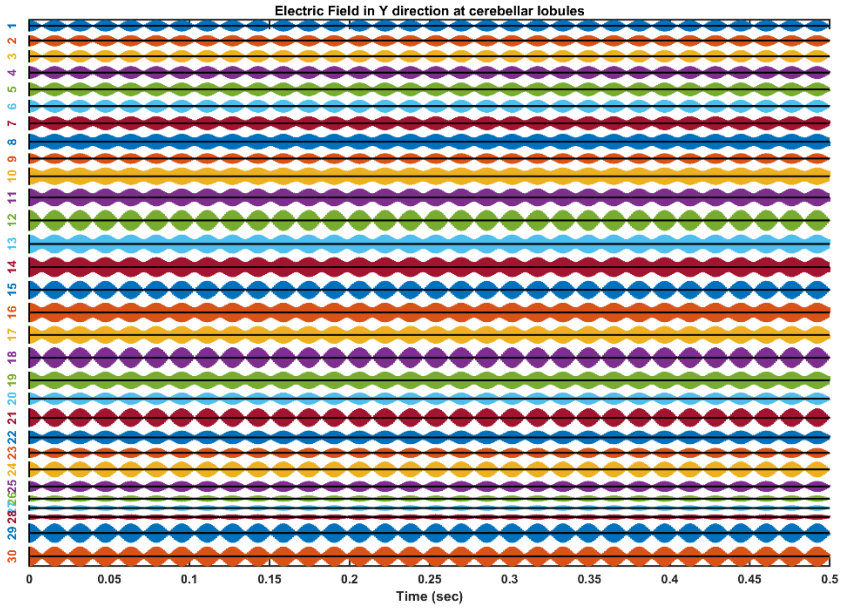

Supplementary Figure S7: tTIS - the resultant mean electric field in Y direction at the cerebellar lobules shows the beats at 63Hz at the dentate nuclei (lobules 29 and 30)

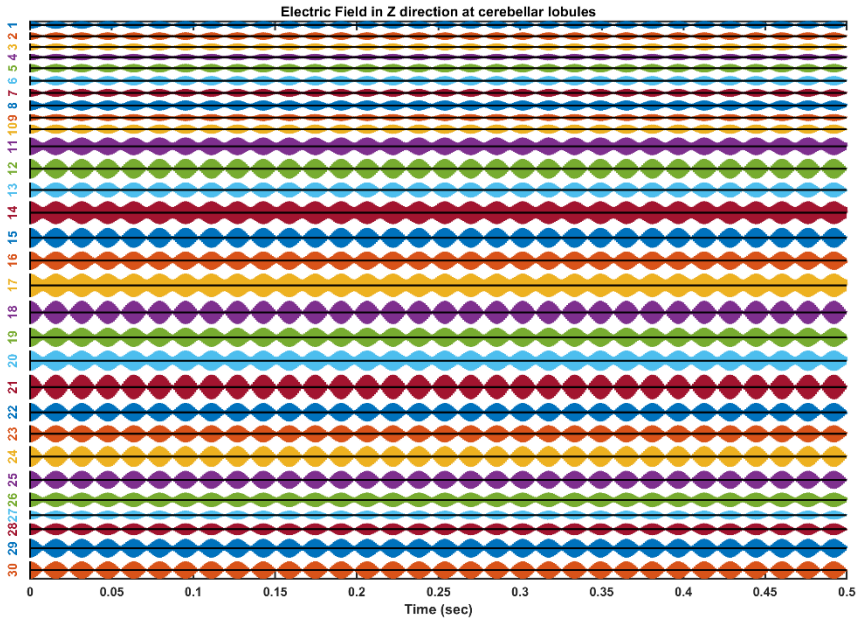

Supplementary Figure S8: tTIS - the resultant mean electric field in Z direction at the cerebellar lobules shows the beats at 63Hz at the dentate nuclei (lobules 29 and 30)

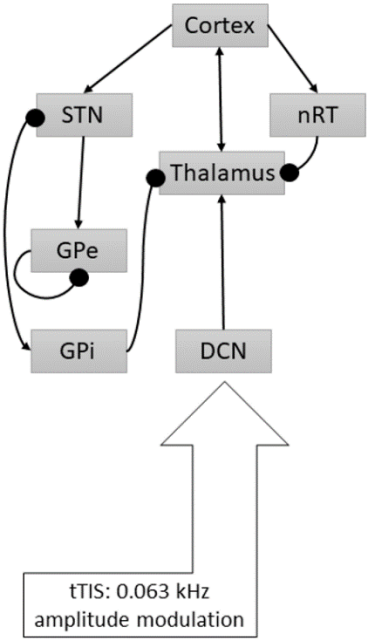

Supplementary Figure S9: Electric field modulation of the deep cerebellar nucleus (DCN) was simulated with the thalamocortical basal ganglia network with DCN from (Yousif et al., 2020) that is presented for tTIS modeling where arrows denote excitatory connections and round arrowheads denote inhibitory connections.

4 Supplementary Figures: fNIRS HbO response to cerebellar tES

Figure S10a shows the average HbO response at prefrontal cortex (PFC) and cerebellum (CER) across subjects due to 2mA ctDCS that led to an increase in the HbO at cerebellar hemispheres as well as a delayed (>150sec) increase in HbO at bilateral PFC. Figure S10b shows the HbO response due to

2mA ctACS where a small change in the HbO was found at the cerebellar hemispheres (fNIRS sensitive to Crus I/II only) while an overall decrease in the HbO was found at the bilateral PFC. However, in the right PFC, HbO response started to increase after 150sec following initial decrease(<150sec).

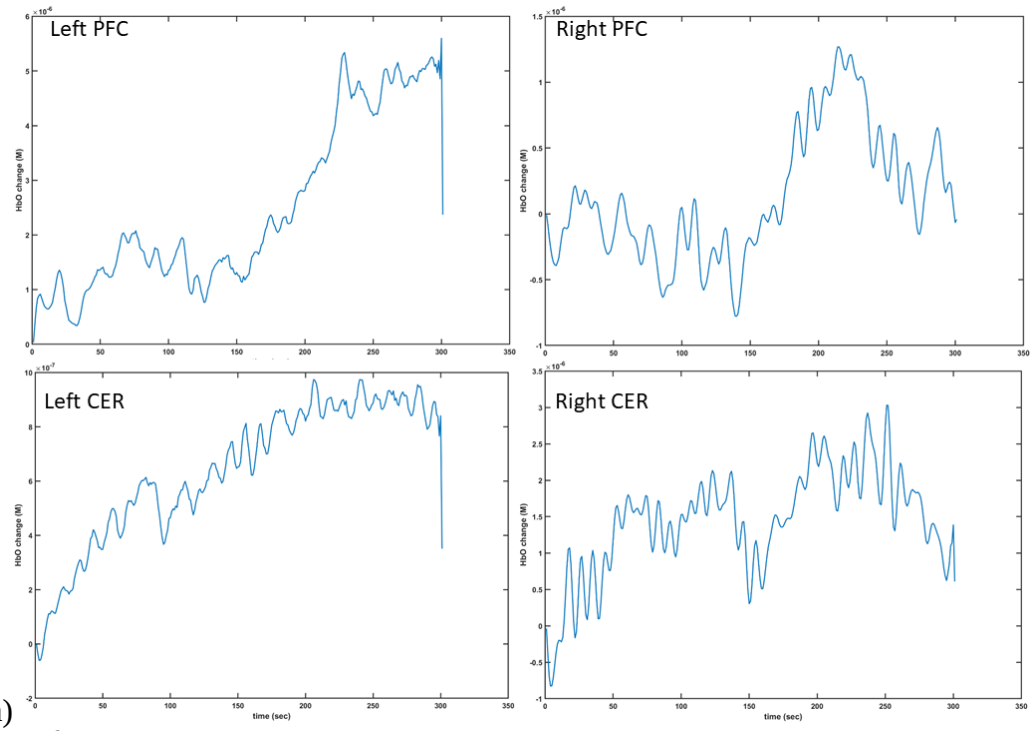

(a)

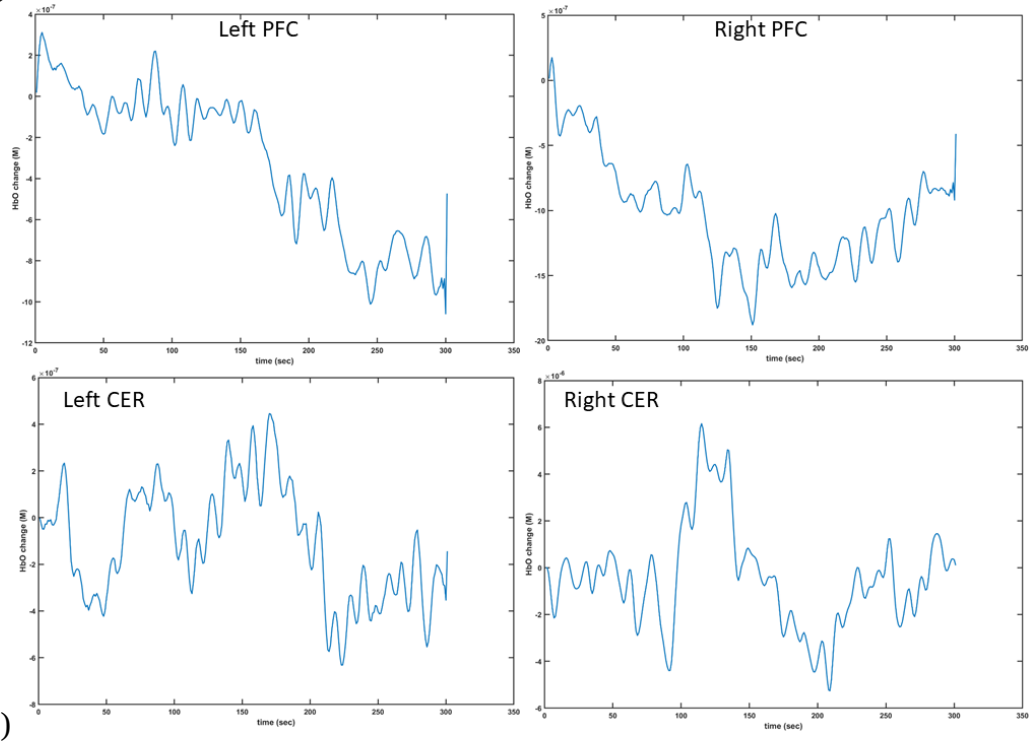

(b)

Supplementary Figure S10: (a) HbO response at the bilateral prefrontal cortex (PFC) and the cerebellum (CER) due to 2mA ctDCS targeting right cerebellar lobules VI-CrusI/II-VIIb (non-motor

representations). (b) HbO response at the bilateral prefrontal cortex (PFC) and the cerebellum (CER) due to 2mA ctACS targeting right cerebellar lobules VI-CrusI/II-VIIb (non-motor representations).

References:

Aasted, C. M., Yücel, M. A., Cooper, R. J., Dubb, J., Tsuzuki, D., Becerra, L., et al. (2015). Anatomical guidance for functional near-infrared spectroscopy: AtlasViewer tutorial. *Neurophotonics* 2, 020801. doi:10.1117/1.NPh.2.2.020801.

Abadi, Z. R. H., and Dutta, A. (2017). Optimizing cerebellar transcranial direct current stimulation for visuomotor learning - anterior versus posterior lobe of cerebellum. in *2017 8th International IEEE/EMBS Conference on Neural Engineering (NER)*, 428–431. doi:10.1109/NER.2017.8008381.

Batsikadze, G., Rezaee, Z., Chang, D.-I., Gerwig, M., Herlitze, S., Dutta, A., et al. (2019). Effects of cerebellar transcranial direct current stimulation on cerebellar-brain inhibition in humans: A systematic evaluation. *Brain Stimulation: Basic, Translational, and Clinical Research in Neuromodulation* 0. doi:10.1016/j.brs.2019.04.010.

Bikson, M., Dmochowski, J., and Rahman, A. (2013). The "quasi-uniform" assumption in animal and computational models of non-invasive electrical stimulation. *Brain Stimul* 6, 704–705. doi:10.1016/j.brs.2012.11.005.

Boyd, S., and Vandenberghe, L. (2004). Convex Optimization by Stephen Boyd. *Cambridge Core*. doi:10.1017/CBO9780511804441.

Dagar, S., Chowdhury, S. R., Bapi, R. S., Dutta, A., and Roy, D. (2016). Near-Infrared Spectroscopy – Electroencephalography-Based Brain-State-Dependent Electrotherapy: A Computational Approach Based on Excitation–Inhibition Balance Hypothesis. *Front Neurol* 7. doi:10.3389/fneur.2016.00123.

Deans, J. K., Powell, A. D., and Jefferys, J. G. R. (2007). Sensitivity of coherent oscillations in rat hippocampus to AC electric fields. *J Physiol* 583, 555–565. doi:10.1113/jphysiol.2007.137711.

Devaney, A. J. (1981). Inverse-scattering theory within the Rytov approximation. *Opt Lett* 6, 374–376. doi:10.1364/ol.6.000374.

Diedrichsen, J. (2006). A spatially unbiased atlas template of the human cerebellum. *Neuroimage* 33, 127–138. doi:10.1016/j.neuroimage.2006.05.056.

Dutta, A., and Nitsche, M. A. (2013). Neural mass model analysis of online modulation of electroencephalogram with transcranial direct current stimulation. in *2013 6th International IEEE/EMBS Conference on Neural Engineering (NER)*, 206–210. doi:10.1109/NER.2013.6695908.

Grossman, N., Bono, D., Dedic, N., Kodandaramaiah, S. B., Rudenko, A., Suk, H.-J., et al. (2017). Noninvasive Deep Brain Stimulation via Temporally Interfering Electric Fields. *Cell* 169, 1029-1041.e16. doi:10.1016/j.cell.2017.05.024.

Grossman, N., Okun, M. S., and Boyden, E. S. (2018). Translating Temporal Interference Brain Stimulation to Treat Neurological and Psychiatric Conditions. *JAMA Neurol* 75, 1307–1308. doi:10.1001/jamaneurol.2018.2760.

Guhathakurta, D., and Dutta, A. (2016). Computational Pipeline for NIRS-EEG Joint Imaging of tDCS-Evoked Cerebral Responses—An Application in Ischemic Stroke. *Front. Neurosci.* 10. doi:10.3389/fnins.2016.00261.

Heeger, D. J. (2017). Theory of cortical function. *Proc Natl Acad Sci U S A* 114, 1773–1782. doi:10.1073/pnas.1619788114.

Huang, Y., Datta, A., Bikson, M., and Parra, L. C. (2017). Realistic vOlumetric-Approach to Simulate Transcranial Electric Stimulation -- ROAST -- a fully automated open-source pipeline. *bioRxiv*, 217331. doi:10.1101/217331.

Ishikawa, T., Tomatsu, S., Tsunoda, Y., Lee, J., Hoffman, D. S., and Kakei, S. (2014). Releasing dentate nucleus cells from Purkinje cell inhibition generates output from the cerebrocerebellum. *PLoS ONE* 9, e108774. doi:10.1371/journal.pone.0108774.

Krienen, F. M., and Buckner, R. L. (2009). Segregated fronto-cerebellar circuits revealed by intrinsic functional connectivity. *Cereb. Cortex* 19, 2485–2497. doi:10.1093/cercor/bhp135.

Lee, S., Lee, C., Park, J., and Im, C.-H. (2020). Individually customized transcranial temporal interference stimulation for focused modulation of deep brain structures: a simulation study with different head models. *Scientific Reports* 10, 11730. doi:10.1038/s41598-020-68660-5.

Meyer, A. F., Williamson, R. S., Linden, J. F., and Sahani, M. (2017). Models of Neuronal Stimulus-Response Functions: Elaboration, Estimation, and Evaluation. *Front Syst Neurosci* 10. doi:10.3389/fnsys.2016.00109.

Mikkonen, M., Laakso, I., Tanaka, S., and Hirata, A. (2020). Cost of focality in TDCS: Interindividual variability in electric fields. *Brain Stimulation* 13, 117–124. doi:10.1016/j.brs.2019.09.017.

Rezaee, Z., and Dutta, A. (2019). A computational pipeline to optimize lobule-specific electric field distribution during cerebellar transcranial direct current stimulation. *Front. Neurosci.* 13. doi:10.3389/fnins.2019.00266.

Rezaee, Z., Kaura, S., Solanki, D., Dash, A., Srivastava, M. V. P., Lahiri, U., et al. (2020). Deep Cerebellar Transcranial Direct Current Stimulation of the Dentate Nucleus to Facilitate Standing Balance in Chronic Stroke Survivors—A Pilot Study. *Brain Sciences* 10, 94. doi:10.3390/brainsci10020094.

Rezaee, Z., Ranjan, S., Solanki, D., Bhattacharya, M., Srivastava, M. V. P., Lahiri, U., et al. (2021). Feasibility of combining functional near-infrared spectroscopy with electroencephalography to identify chronic stroke responders to cerebellar transcranial direct current stimulation-a computational modeling and portable neuroimaging methodological study. *Cerebellum*. doi:10.1007/s12311-021-01249-4.

ROGERS, T. D., DICKSON, P. E., HECK, D. H., GOLDOWITZ, D., MITTLEMAN, G., and BLAHA, C. D. (2011). Connecting the Dots of the Cerebro-Cerebellar Role in Cognitive Function: Neuronal Pathways for Cerebellar Modulation of Dopamine Release in the Prefrontal Cortex. *Synapse* 65. doi:10.1002/syn.20960.

Rolls, E. T., Huang, C.-C., Lin, C.-P., Feng, J., and Joliot, M. (2020). Automated anatomical labelling atlas 3. *NeuroImage* 206, 116189. doi:10.1016/j.neuroimage.2019.116189.

Saturnino, G. B., Puonti, O., Nielsen, J. D., Antonenko, D., Madsen, K. H. H., and Thielscher, A. (2018). SimNIBS 2.1: A Comprehensive Pipeline for Individualized Electric Field Modelling for Transcranial Brain Stimulation. *bioRxiv*, 500314. doi:10.1101/500314.

Schacht, J. P., Anton, R. F., and Myrick, H. (2013). Functional neuroimaging studies of alcohol cue reactivity: a quantitative meta-analysis and systematic review. *Addict Biol* 18, 121–133. doi:10.1111/j.1369-1600.2012.00464.x.

Schulman, J. J., Cancro, R., Lowe, S. I., Lu, F., Walton, K. D., and Llinás, R. R. (2011). Imaging of Thalamocortical Dysrhythmia in Neuropsychiatry. *Front. Hum. Neurosci.* 5. doi:10.3389/fnhum.2011.00069.

Shin, S.-L., and De Schutter, E. (2006). Dynamic Synchronization of Purkinje Cell Simple Spikes. *Journal of Neurophysiology* 96, 3485–3491. doi:10.1152/jn.00570.2006.

Yousif, N., Bain, P. G., Nandi, D., and Borisyuk, R. (2020). A Population Model of Deep Brain Stimulation in Movement Disorders From Circuits to Cells. *Front. Hum. Neurosci.* 14. doi:10.3389/fnhum.2020.00055.

Zhang, X., and Santaniello, S. (2019). Role of cerebellar GABAergic dysfunctions in the origins of essential tremor. *PNAS* 116, 13592–13601. doi:10.1073/pnas.1817689116.